Transfer Learning Assisted Parameter Selection for Water-Fat Separation in Dixon MRI

Alan Okinaka
Physics Department,
Ursinus College
Collegeville, PA 19426
alokinaka@ursinus.edu

Gulfam Ahmed Saju
Computer and Information
Science Department, University
of Massachusetts Dartmouth
North Dartmouth, MA 02747
gsaju@umassd.edu

Yuchou Chang
Computer and Information
Science Department, University
of Massachusetts Dartmouth
North Dartmouth, MA 02747
ychang1@umassd.edu

***Abstract*— The Dixon method is a clinical Magnetic Resonance Imaging (MRI) approach employed to differentiate and separate water and fat signals and plays a crucial role in various clinical applications. The efficiency of this method is largely influenced by the optimal selection of parameters such as Echo Time (TE) and Echo Spacing. However, acquiring these optimal parameters can be challenging due to the limited availability of training datasets and the complexity of manual selection. This study proposes a novel parameter selection method using transfer learning on simulated images to address these challenges. We leverage pre-trained models trained on one task as a starting point for a related task, under the framework of transfer learning. This approach helps identify optimal TE and echo spacing parameters and thus aids in optimizing Dixon technique parameters. Our proposed method customizes these models to the specific task of differentiating water-only or fat-only images. Experimental results reveal that these pre-trained models can successfully classify the simulated images, thereby providing promising implications for enhancing the performance of the Dixon method in MRI.**

Keywords— Magnetic Resonance Imaging, Efficient-Net, MobileNet, SqueezeNet, Water-Fat Separation, Transfer Learning.

I. INTRODUCTION

The Dixon method [4], a clinical Magnetic Resonance Imaging (MRI) approach, plays a vital role in differentiating and separating water and fat signals. It has gained substantial traction and is widely used in various clinical applications due to its robust and insightful outcomes. The Dixon method takes advantage of the phase difference between the hydrogen in water and fat molecules, there is a phase difference between the molecules since their protons' precess at different times [30, 35].

The parameters of the echos itself can greatly affect the quality of the final water-fat separation image [17]. Echo Time (TE), the interval between the application of the radio frequency (RF) pulse and the peak of the echo signal, plays a pivotal role in determining the phase difference between water and fat signals. Meanwhile, Echo Spacing representing the time gap between successive echoes in a multi-echo sequence also holds critical importance. It can directly influence the quality of fat-water separation by affecting the amount of T2* decay that occurs between echoes. T2* decay inevitably leads to signal loss. Consequently, shorter echo spacing has the potential to minimize this decay and enhance the quality of images[1]. However, excessively short echo spacing can also introduce complications, such as distortions stemming from magnetic field inhomogeneities, underscoring the need for careful calibration of these parameters to optimize the performance of the Dixon method in MRI.

The quality of the images that are produced from the Dixon method for water-fat separation in MRI is dependent on the judicious selection of echo parameters. Since there are so many parameters to choose from deep learning methods have potential in assisting with the optimization of these echo parameters [34]. We can do this by using Deep Neural Networks (DNN) [28] to learn from large the data sets of images to find the best possible echo configurations. By finding the best echo configurations we can produce better quality Dixon images. The complication we run into is to use DNN we need large sets of training data and in this case, they are Dixon images. Since the images for training are medical images for legal reasons, we do not have access to large sets of these photos. Instead, we will simulate the image, and through simulation we are able to create a large and diverse set of training data to use in our DNN.

The DNN we are putting these images through are pre-trained models and we used transfer learning on each of them with our own test set. The utilization of pre-trained models could offer valuable insights to determine parameters for simulated water or fat images. Transfer learning, a machine learning strategy that leverages pre-existing models trained on one task as a starting point for a related task, emerges as a potential solution for identifying optimal parameters [27, 31]. For example, binary classification of water images versus fat images can lead to the discovery of optimal TE and echo spacing parameters.

In this paper, we propose a novel transfer learning approach aimed at identifying the Dixon parameters using pre-trained models. Our method leverages the robustness of these models and customizes them to the specific task of differentiating water and fat images, thus aiding in the optimization of Dixon technique parameters. This paper is structured as follows to present our findings: the first section serves as an introduction, setting the context, and presenting the problem. The second part discusses the current landscape of solutions and related works.

The third section provides a detailed description of our proposed transfer learning method, specifically tailored for classifying water-only images or fat-only images. The fourth section unveils the experimental results, demonstrating the efficacy of our proposed method. Finally, the fifth section concludes the paper, summarizing our findings, their implications for identifying Dixon parameters, and the potential directions for further research.

II. Related Works

The Dixon water and fat signal separation MRI technique has a vast spectrum of clinical applications. One application is enhancing tissue contrast especially when the fat and water is intermingled in certain parts of the body. Some examples where fat and water is intermingled is in the liver [3], pancreas, and breasts[14, 18]. Also in the liver we can quantify fat [2] and also identify lesions or disease [19, 6]. The Dixon method can also apply to musculoskeletal imaging [15, 1], and we can use it to detect rheumatoid arthritis [13]. Thus the Dixon method's many clinical applications make it a very important tool to optimize.

The versatility of the Dixon method stems from its ability to separate fat and water with high precision, making it valuable for a wide range of diagnostic purposes. In liver imaging, for instance, it provides a non-invasive approach for assessing hepatic steatosis and monitoring fat deposition, which is crucial in managing metabolic diseases. In oncology, Dixon imaging helps identify and characterize lesions that may be masked by fat tissue, improving tumor detection and treatment planning [6]. Its application in musculoskeletal imaging allows for detailed analysis of fat infiltration in muscles, which is important for evaluating degenerative conditions and assessing therapeutic outcomes [15]. Furthermore, Dixon techniques are increasingly being used in cardiac imaging [29], particularly for detecting epicardial fat and its implications in cardiovascular diseases [13].

III. Proposed Method

The Dixon method leverages the difference in the precession frequencies of fat and water to separate them in the resultant images. Given that fat and water resonate at slightly different frequencies, they will be in-phase or out-of-phase at different TE. The basic Dixon method requires at least two echoes, typically collected at in-phase and out-of-phase timings. In mathematical terms, this can be represented as follows. When the water and fat signals add together, the in-phase image can be represented as

$$I\_IP = W + F \tag{1}$$

, where I_IP is the in-phase image, W represents the water signal, and F represents the fat signal. When the water and fat signals are subtracted, the out-of-phase image is represented as

$$I\_OP = W - F \tag{2}$$

, where I_OP is the out-phase image. By using these two equations, we can isolate the water and fat signals:

$$W = (I\_IP + I\_OP)/2 \tag{3}$$

, and

$$F = (I\_IP - I\_OP)/2 \tag{4}$$

. These are the forms of the Dixon equations, assuming a 2-point Dixon method, which is the most basic form of the method. They do not take into account factors such as T2* decay, B0 inhomogeneities [23, 24], or the multiple spectral peaks of fat, which can complicate matters. In more advanced versions of the method (like 3-point Dixon or iterative Dixon), additional acquisitions and more complex calculations are used to address these issues.

A. Simulation Tool

QMRITools developed by Martijn Froeling [5] is a comprehensive toolbox written in Mathematica using Wolfram Workbench and Eclipse [12]. It's designed for processing quantitative MRI data without the use of a graphical user interface (GUI) which focuses primarily on facilitating rapid and batch data processing. In addition, it supports the development and prototyping of new functions. The toolbox's core is packed with numerous functions for data manipulation and restructuring, making it an efficient resource for quantitative MRI data analysis. Originally created for analyzing diffusion imaging data of skeletal muscles, QMRITools' functionality has exponentially expanded over the years. It is currently employed for the analysis, processing, and simulations of quantitative muscle, nerve, and cardiac MRI and spectroscopy data. As research evolves, so does the library of functions within the toolbox, reflecting its dynamic and versatile nature. We used the QMRITools for simulating Dixon method in MRI.

Utilizing QMRITools, we successfully simulated the Dixon method to generate distinct water and fat images, as depicted in Fig. 1. The water-only images of legs are represented in Fig. 1(a), and the fat-only images in Fig. 1(b). They clearly demonstrate that the fat components are located externally to the water components on the legs. The marrow components inside water tissues represent fat parts, so they have stronger signals in fat images and weak signals in water images. This separation of water and fat allows for an enhanced diagnostic perspective, potentially improving patient outcomes. As part of our ongoing analysis, we aim to generate multiple pairs of these water and fat images, adjusting parameters such as TE and echo spacing to further optimize the clarity and diagnostic value of the images.

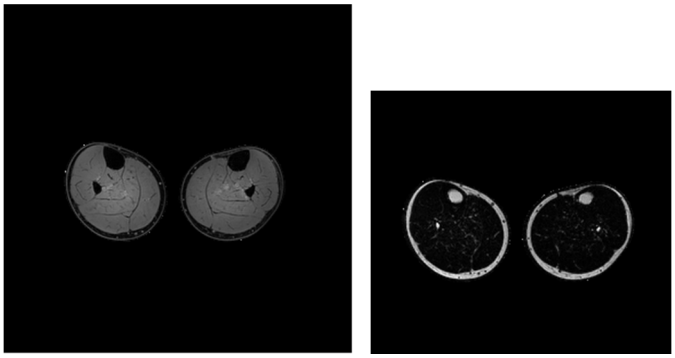

(a). Water-Only Image (b). Fat-Only Image

Fig. 1. Simulated water-only and fat-only images of legs from QMRITools. The left figure represents water images, and the right figure denotes fat images. It is seen that the fat images are outside of water components on legs. In addition, marrow tissues represent fat components so they have strong signals in fat images and weak signals in water images.

B. Generation of water and fat image training data

Pre-processing data for our experiment can be divided into several steps, which include importing the necessary toolbox, creating images with various parameters, saving these images in

a specific format, and finally converting them to a more commonly used format. The first step of pre-processing the data involves importing the QMRITools toolbox since it contains a host of functions that are mandatory for simulating MRI images. After importing the toolbox we use a double for loop to create images with different parameters. Next we use a double 'For' loop to create images with different echo spacing's and TE's. A loop is a control flow statement that allows the image simulation to be executed repeatedly automatically. A nested loop allows to iterate over multiple dimensions, which in this context means systematically changing both the echo spacing's and initial echo times. By setting a range of both of these parameters we can generate a lot of images with many different parameters. After generating the images they are saved locally to our local drive for ease of access. Finally, we convert the recently saved images from Nifti format to Portable Network Graphics(PNG) format. Nifti is a commonly used format for storing neuroimaging data sets and is commonly used in the field of MRI. The images are being converted to PNG format since the images can be more easily viewed and shared to other people and artificial intelligence models.

After we have the images in PNG format we then need to generate training data so our DNN can learn from the training data set. First we use a loop to create each of the labels for the all the individual images created. Adding labels to your data is important since it will provide the artificial intelligence with information about the data given to it. The labels in our case are binary which means there are two classes, but there can even be multi-class or even more complex labels depending on the experiment. the next step involves a triple nested loop over a range of echo spacing, initial echo times, and a list of pre-trained models. The aim of this iterative process is to train each pre-trained model with different sets of echo spacing and initial echo times. This comprehensive approach ensures that our models are thoroughly trained across a variety of scenarios, which can contribute to a more robust performance. Once the models are trained with various parameters, the next step is to apply the labels to .png images of either water or fat scans. Labeling is crucial in supervised learning as it allows the model to learn the relationship between the input (images) and the output (labels).

C. *Thresholding classes of binary classification via pre-trained models*

In our experimental approach, we implemented a manual threshold on echo times and echo spacing to classify water or fat images into two respective classes. This binning strategy was integral to the establishment of a framework for evaluating the performance of various classification methods. Each class representing a range of echo times or echo spacings was labeled for this evaluative process. Given the practical challenges associated with procuring a sizeable amount of training data for water and fat images from Dixon methods in clinical settings, our approach pivoted towards utilizing existing pre-trained models. We chose to use a range of models, including DenseNet-121 [10], Efficient-Net [22], EfficientNet-V2 [36], Inception V3[21], MobileNet V3[8], ResNet-101[7], ResNet-152 [7], ResNet-50[7], ShuffleNet-V2 [16], Squeeze-and-Excitation Net [9], SqueezeNet V1.1 [11], VGG-16 [20], and VGG-19 [20]. The decision to use pretrained models capitalizes on the wealth of learning these models have acquired from large-scale training data and allows us to circumvent the difficulty of generating our own exhaustive data set.

Subsequent to the classification process using these pre-trained models, we collected classification accuracy for each model. The metric of accuracy serves as an objective measure of the performance of each pre-trained model, providing a quantitative basis to compare and analyze their efficacy. It's noted that our approach involves a manually determined threshold on the echo times and echo spacing. This threshold isn't a rigid and unchanging element. Instead, it can be modulated to facilitate a comprehensive evaluation. This capacity to adjust the threshold ensures a flexible and robust evaluation, enabling a more thorough understanding of the relationship between the Dixon parameters and the classification performance.

D. *Apply transfer learning to the model*

After being labeled we apply transfer learning to the pre-trained models. Transfer learning is a machine learning method where we use a pre-trained model's DNN architecture to train our own labeled images on the DNN. This process allows us to leverage the learned features of the pre-trained model, saving computation time and potentially improving performance. Finally, we calculate the classifier measurement. This measurement evaluates the performance of the model in accurately predicting labels. Common measurements include accuracy, precision, recall, and F1 score. This evaluation step is essential to understand how well our model is performing and to identify areas for potential improvement. These steps represent a systematic approach to generating training data for transfer learning, providing a strong foundation for creating robust and efficient machine learning models.

IV. Experimental Results

A. *Data sets*

We simulated four echo dixon method images where we only changed the initial echo and the set of images created satisfy a range of initial echos from 2 ms to 3.5 ms and a range of echo spacing's (e.g. times between each echo) is from 0.7 ms to 1.7 ms. We generated 1517 pairs of water and fat images where a few examples are show in Fig. 2. Changing these parameters created a large set of images that all have unique information that could be put into the models. Due to computational performance constraints only 1000 out of the 1517 images were trained on each of the models. Also, excluding the 1000 pairs trained on each model there where 17 pairs out of the 517 left that were used to record a classification score measurement.

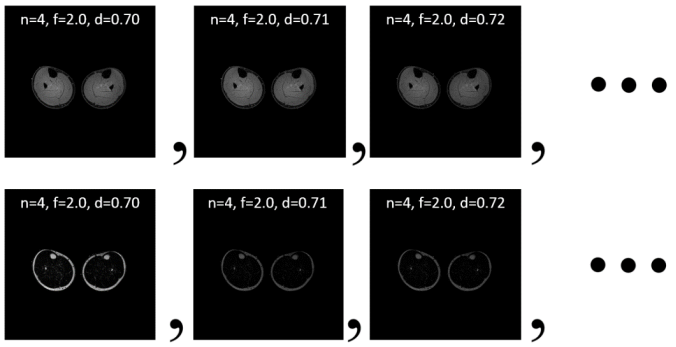

Fig. 2. Through changing Dixon parameters including echo times and echo spacing, a sequence of water and fat images is generated. Here, n represents the amount of echoes, f denotes the initial echo, and d represents the time between each echo. Both the initial echo and the time between each echo has units of milliseconds.

B. Classification performance

The overall mean classification measurement for all models as shown in Fig. 5. Two out of the eighteen models tested came out to have the best on average classification score even though all models have a mean classification score above 55%. Squeeze-and-Excitation Net and ShuffleNet-V2 both got a score of 70% which is at most 15% more than the other models.

We also decided to look at the fat image classification measurement means as shown in Fig. 3 and the water image classification means in Fig. 4. First after collecting the fat image means we found that the two models that had the highest overall mean classification measurement have the highest classification measurement for both echo spacing and TE. Also both models exchange the prominent classification measurement in both echo spacing and echo spacing.

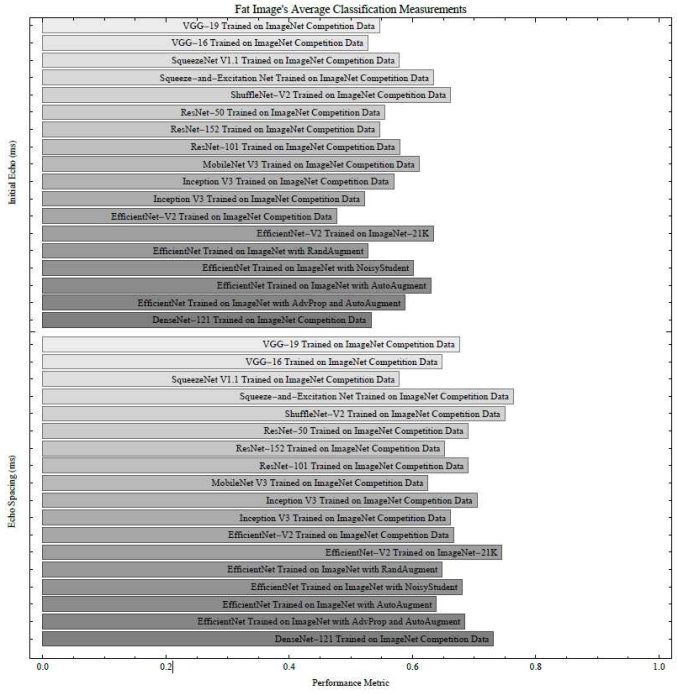

Fig. 3. The following figure shows the collected means of all classification measurements by models are optimizing the initial echo (ms) and the echo spacing (ms) of fat images. The length of each of the model's bars is a qualitative representation of the models means. All models had better optimization results identifying the fat images over a range of echo spacings (ms) compared to initial echos.

The water image classification measurements show EfficientNet and Inception V3 DNN models having the highest mean classification score. Which is different from the two models that got the highest overall mean classification score. A similarity between the water classification measurement means and the fat classification measurement means is echo spacing has shown a general higher score compared to initial echo.

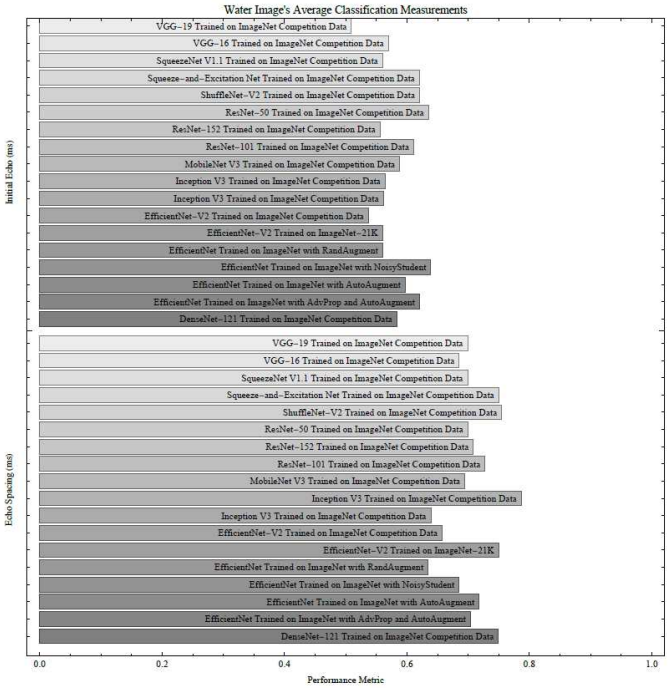

Fig. 4. The following figure shows the collected means of all classification measurements by models are optimizing the initial echo (ms) and the echo spacing (ms) of water images. The length of each of the model's bars is a qualitative representation of the models means. All models had better optimization results identifying the water images over a range of echo spacings (ms) compared to initial echos.

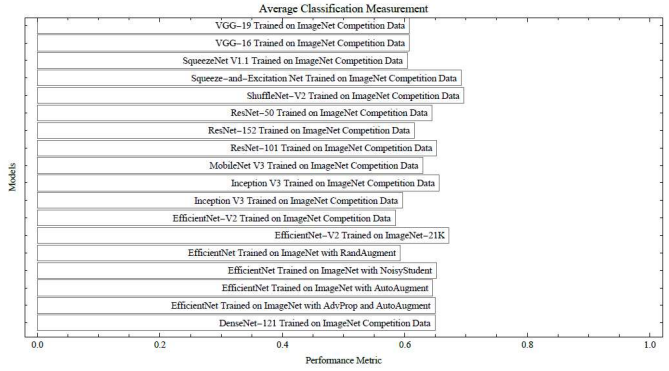

Fig. 5. The figure shows a bar graph of the mean over all classification measurements collected from each model. Each bar is labeled signifying each model and the length of each bar represents the performance metric.

V. CONCLUSION

The models we tested all had a feasible average classification measurement greater than or equal to 59%, two of the models had the best average classification measurement which was

Squeeze-and-Excitation Net and ShuffleNet-V2. This means both of these models are a viable option for identifying parameters of a Dixon image which can be further applicable to being used in further Dixon echo optimization experiments. Further we are planning to use a larger range of parameters and see if these two image classification models are good with a higher or lower range of initial echos and echo spacing's. We will also try further testing in python with a wider range of pre-trained models to compare and see if there are any other models that are much more suitable for parameter selection for Dixon MRI water-fat separation.

ACKNOWLEDGMENT

This work was supported by the National Science Foundation under Grant No. 2050972.

REFERENCES

[1] Afsahi, A.M., Ma, Y., Jang, H., Jerban, S., Chung, C.B., Chang, E.Y., Du, J.: Ultrashort Echo Time Magnetic Resonance Imaging Techniques: Met and Unmet Needs in Musculoskeletal Imaging. Journal of Magnetic Resonance Imaging 55(6), 1597–1612 (2022). https://doi.org/10.1002/jmri.28032, https://onlinelibrary.wiley.com/doi/abs/10.1002/jmri.28032.

[2] Brancato, V., Della Pepa, G., Bozzetto, L., Vitale, M., Annuzzi, G., Basso, L., Cavaliere, C., Salvatore, M., Rivellese, A.A., Monti, S.: Evaluation of a Whole-Liver Dixon-Based MRI Approach for Quantification of Liver Fat in Patients with Type 2 Diabetes Treated with Two Isocaloric Different Diets. Diagnostics 12(2), 514 (Feb 2022). https://doi.org/10.3390/diagnostics12020514, https://www.mdpi.com/2075-4418/12/2/514, number: 2 Publisher: Multidisciplinary Digital Publishing Institute.

[3] Ding, Y., Rao, S.X., Chen, C.Z., Li, R.C., Zeng, M.S.: Usefulness of two-point Dixon fat-water separation technique in gadoxetic acid-enhanced liver magnetic resonance imaging. World Journal of Gastroenterology : WJG 21(16), 5017–5022 (Apr 2015). https://doi.org/10.3748/wjg.v21.i16.5017, https://www.ncbi.nlm.nih.gov/pmc/articles/PMC4408476/.

[4] Dixon, W.T.: Simple proton spectroscopic imaging. Radiology 153(1), 189–194 (Oct 1984). https://doi.org/10.1148/radiology.153.1.6089263

[5] Froeling, M.: QMRTools: a Mathematica toolbox for quantitative MRI analysis. Journal of Open Source Software 4(38), 1204 (Jun 2019). https://doi.org/10.21105/joss.01204, https://joss.theoj.org/papers/10.21105/joss.01204.

[6] Hayashi, T., Saitoh, S., Takahashi, J., Tsuji, Y., Ikeda, K., Kobayashi, M., Kawamura, Y., Fujii, T., Inoue, M., Miyati, T., Kumada, H.: Hepatic fat quantification using the two-point Dixon method and fat color maps based on non-alcoholic fatty liver disease activity score. Hepatology Research 47(5), 455–464 (2017). https://doi.org/10.1111/hepr.12767, https://onlinelibrary.wiley.com/doi/abs/10.1111/hepr.12767.

[7] He, K., Zhang, X., Ren, S., Sun, J.: Deep Residual Learning for Image Recognition (Dec 2015). https://doi.org/10.48550/arXiv.1512.03385, http://arxiv.org/abs/1512.03385, arXiv:1512.03385 [cs].

[8] Howard, A., Sandler, M., Chu, G., Chen, L.C., Chen, B., Tan, M., Wang, W., Zhu, Y., Pang, R., Vasudevan, V., Le, Q.V., Adam, H.: Searching for MobileNetV3 (Nov 2019). https://doi.org/10.48550/arXiv.1905.02244, http://arxiv.org/abs/1905.02244, arXiv:1905.02244 [cs].

[9] Hu, J., Shen, L., Albanie, S., Sun, G., Wu, E.: Squeeze-and-Excitation Networks (May 2019). https://doi.org/10.48550/arXiv.1709.01507, http://arxiv.org/abs/1709.01507, arXiv:1709.01507 [cs].

[10] Huang, G., Liu, Z., van der Maaten, L., Weinberger, K.Q.: Densely Connected Convolutional Networks (Jan 2018). https://doi.org/10.48550/arXiv.1608.06993, http://arxiv.org/abs/1608.06993, arXiv:1608.06993 [cs] version: 5.

[11] Iandola, F.N., Han, S., Moskewicz, M.W., Ashraf, K., Dally, W.J., Keutzer, K.: SqueezeNet: AlexNet-level accuracy with 50x fewer parameters and <0.5MB model size (Nov 2016). https://doi.org/10.48550/arXiv.1602.07360, http://arxiv.org/abs/1602.07360, arXiv:1602.07360 [cs].

[12] Inc., W.R.: Mathematica, Version 13.3, https://www.wolfram.com/mathematica, champaign, IL, 2023.

[13] Kirchgesner, T., Stoenoiu, M., Durez, P., Michoux, N., Vande Berg, B.: MRI of Hands with Early Rheumatoid Arthritis: Usefulness of Three-Point Dixon Sequences to Quantitatively Assess Disease Activity. Journal of the Belgian Society of Radiology 106(1), 1. https://doi.org/10.5334/jbsr.2692, https://www.ncbi.nlm.nih.gov/pmc/articles/PMC8757386/.

[14] Le, Y., Kipfer, H., Majidi, S., Holz, S., Dale, B., Geppert, C., Kroeker, R., Lin, C.: Application of time-resolved angiography with stochastic trajectories (twist)-dixon in dynamic contrast-enhanced (dce) breast mri. Journal of Magnetic Resonance Imaging 38(5), 1033–1042 (2013). https://doi.org/10.1002/jmri.24062, https://onlinelibrary.wiley.com/doi/abs/10.1002/jmri.24062.

[15] Ma, J.: Dixon techniques for water and fat imaging. Journal of Magnetic Resonance Imaging 28(3), 543–558 (2008). https://doi.org/10.1002/jmri.21492, https://onlinelibrary.wiley.com/doi/abs/10.1002/jmri.21492.

[16] Ma, N., Zhang, X., Zheng, H.T., Sun, J.: ShuffleNet V2: Practical Guidelines for Efficient CNN Architecture Design (Jul 2018). https://doi.org/10.48550/arXiv.1807.11164, http://arxiv.org/abs/1807.11164.

[17] Pezeshk, P., Alian, A., Chhabra, A.: Role of chemical shift and Dixon based techniques in musculoskeletal MR imaging. European Journal of Radiology 94, 93–100 (Sep 2017). https://doi.org/10.1016/j.ejrad.2017.06.011, https://www.sciencedirect.com/science/article/pii/S0720048X17302589.

[18] Saranathan, M., Rettmann, D.W., Hargreaves, B.A., Lipson, J.A., Daniel, B.L.: Variable spatiotemporal resolution three-dimensional dixon sequence for rapid dynamic contrast-enhanced breast MRI. Journal of Magnetic Resonance Imaging 40(6), 1392–1399 (2014). https://doi.org/10.1002/jmri.24490, https://onlinelibrary.wiley.com/doi/abs/10.1002/jmri.24490.

[19] Shi, G.Z., Chen, H., Zeng, W.K., Gao, M., Wang, M.Z., Zhang, H.T., Shen, J.: R2* value derived from multi-echo Dixon technique can aid discrimination between benign and malignant focal liver lesions. World Journal of Gastroenterology 27(12), 1182–1193 (Mar 2021). https://doi.org/10.3748/wjg.v27.i12.1182, https://www.ncbi.nlm.nih.gov/pmc/articles/PMC8006098/.

[20] Simonyan, K., Zisserman, A.: Very Deep Convolutional Networks for Large-Scale Image Recognition (Apr 2015). https://doi.org/10.48550/arXiv.1409.1556, http://arxiv.org/abs/1409.1556, arXiv:1409.1556 [cs] version: 6.

[21] Szegedy, C., Vanhoucke, V., Ioffe, S., Shlens, J., Wojna, Z.: Rethinking the Inception Architecture for Computer Vision (Dec 2015). https://doi.org/10.48550/arXiv.1512.00567, http://arxiv.org/abs/1512.00567, arXiv:1512.00567 [cs] version: 3.

[22] Tan, M., Le, Q.V.: EfficientNet: Rethinking Model Scaling for Convolutional Neural Networks (Sep 2020). https://doi.org/10.48550/arXiv.1905.11946, http://arxiv.org/abs/1905.11946, arXiv:1905.11946 [cs, stat] version: 5.

[23] Matakos, A., Balter, J., & Cao, Y. (2014). Estimation of geometrically undistorted B0 inhomogeneity maps. Physics in Medicine & Biology, 59(17), 4945.

[24] Roberts, N. T., Hinshaw, L. A., Colgan, T. J., Ii, T., Hernando, D., & Reeder, S. B. (2021). B0 and B1 inhomogeneities in the liver at 1.5 T and 3.0 T. Magnetic resonance in medicine, 85(4), 2212-2220.

[25] Basty, N., Thanaj, M., Cule, M., Sorokin, E. P., Liu, Y., Thomas, E. L., ... & Whitcher, B. (2023). Artifact-free fat-water separation in Dixon MRI using deep learning. Journal of Big Data, 10(1), 4.

[26] Smith, A. K., Dortch, R. D., Dethrage, L. M., Lyttle, B. D., Kang, H., Welch, E. B., & Smith, S. A. (2017). Incorporating Dixon multi - echo fat water separation for novel quantitative magnetization transfer of the human optic nerve in vivo. Magnetic resonance in medicine, 77(2), 707-716.

[27] Torrey, L., & Shavlik, J. (2010). Transfer learning. In Handbook of research on machine learning applications and trends: algorithms, methods, and techniques (pp. 242-264). IGI global.

[28] Miikkulainen, R., Liang, J., Meyerson, E., Rawal, A., Fink, D., Francon, O., ... & Hodjat, B. (2024). Evolving deep neural networks. In Artificial intelligence in the age of neural networks and brain computing (pp. 269-287). Academic Press.

[29] Zeilinger, M. G., Wiesmüller, M., Forman, C., Schmidt, M., Munoz, C., Piccini, D., ... & Wuest, W. (2021). 3D Dixon water-fat LGE imaging with image navigator and compressed sensing in cardiac MRI. European Radiology, 31, 3951-3961.

[30] Basty, N., Thanaj, M., Cule, M., Sorokin, E. P., Liu, Y., Bell, J. D., ... & Whitcher, B. (2021). Swap-free fat-water separation in Dixon MRI using conditional generative adversarial networks. arXiv preprint arXiv:2107.14175.

[31] Zhuang, F., Qi, Z., Duan, K., Xi, D., Zhu, Y., Zhu, H., ... & He, Q. (2020). A comprehensive survey on transfer learning. Proceedings of the IEEE, 109(1), 43-76.

[32] Wang, H., Liang, D., King, K. F., Nagarsekar, G., Chang, Y., & Ying, L. (2012). Improving GRAPPA using cross - sampled autocalibration data. Magnetic Resonance in Medicine, 67(4), 1042-1053.

[33] Chang, Y., Liang, D., & Ying, L. (2012). Nonlinear GRAPPA: A kernel approach to parallel MRI reconstruction. Magnetic Resonance in Medicine, 68(3), 730-740.

[34] Chang, Y., Li, Z., Saju, G., Mao, H., & Liu, T. (2023). Deep learning-based rigid motion correction for magnetic resonance imaging: a survey. Meta-Radiology, 100001.

[35] Schär, M., Eggers, H., Zwart, N. R., Chang, Y., Bakhru, A., & Pipe, J. G. (2016). Dixon water - fat separation in PROPELLER MRI acquired with two interleaved echoes. Magnetic resonance in medicine, 75(2), 718-728.

[36] Tan, M., Le, Q.V.: EfficientNetV2: Smaller Models and Faster Training (Jun 2021). https://doi.org/10.48550/arXiv.2104.00298, http://arxiv.org/abs/2104.00298, arXiv:2104.00298 [cs] version: 3.